In §6, we examine the form of strain-energy function constructed with reference to inequalities that ensure 'physically reasonable response', including the monotonicity of the stress deformation behaviour in uniaxial tests and notions of convexity and strong ellipticity in three dimensions. These all require, in particular, that the material constants included in various terms contributing to the strain energy are positive, which is consistent with the values obtained in fitting the data. Finally, §7 is devoted to a concluding discussion.

2. Morphology, structure and typical mechanical behaviour of the passive myocardium

(*a*) *Morphology and structure*

The human heart consists of four chambers, namely the right and left *atria*, which receive blood from the body, and the left and right *ventricles*, which pump blood around the body. For a detailed description of the individual functionalities of these four chambers, see Katz (1977). There is still an ongoing debate concerning the structure of the heart (Gilbert *et al.* 2007), and, in particular, the anisotropic cardiac microstructure. One approach describes the heart as a single muscle coiled in a helical pattern, whereas the other approach considers the heart to be a continuum composed of laminar sheets, an approach we are adopting in the present work.

The left ventricle has the largest volume of the four chambers and serves the particular purpose of distributing blood with a higher pressure than the right ventricle. As a consequence of the need to support higher pressure, the wall thickness of the left ventricle is larger than that of the right ventricle. The wall thickness and curvature of the left ventricle vary spatially; it is thickest at the base and at the equator, and thinnest at its apex. The wall thickness and curvature also vary temporally through the cardiac cycle. The left ventricular wall may be regarded as a continuum of myocardial fibres, with a smooth transmural variation of the fibre orientations. It is modelled reasonably well as a thick-walled ellipsoid of revolution that is truncated at the base, as depicted in figure 1*a*.

The heart wall consists of three distinct layers: an inner layer (the *endocardium*), a middle layer (the *myocardium*) and an outer layer (the *epicardium*). The endocardium lines the inside of the four chambers and it is a serous membrane, with approximate thickness 100 μm, consisting mainly of epimysial collagen, elastin and a layer of endothelial cells, the latter serving as an interfacial layer between the wall and the blood. The protective epicardium is also a membrane with thickness of the order of 100 μm and consists largely of epimysial collagen and some elastin.

In this paper, we focus our attention on the myocardium of the left ventricle. The ventricular myocardium is the functional tissue of the heart wall with a complex structure that is well represented in the quantitative studies of LeGrice *et al.* (1995, 1997), Young *et al.* (1998) and Sands *et al.* (2005). The left ventricular wall is a composite of layers (or sheets) of parallel myocytes, which are the predominant fibre types, occupying about 70 per cent of the volume. The remaining 30 per cent consists of various interstitial components (Frank & Langer 1974), whereas only 2–5 per cent of the interstitial volume is occupied by collagen arranged in a spatial network that forms lateral connections

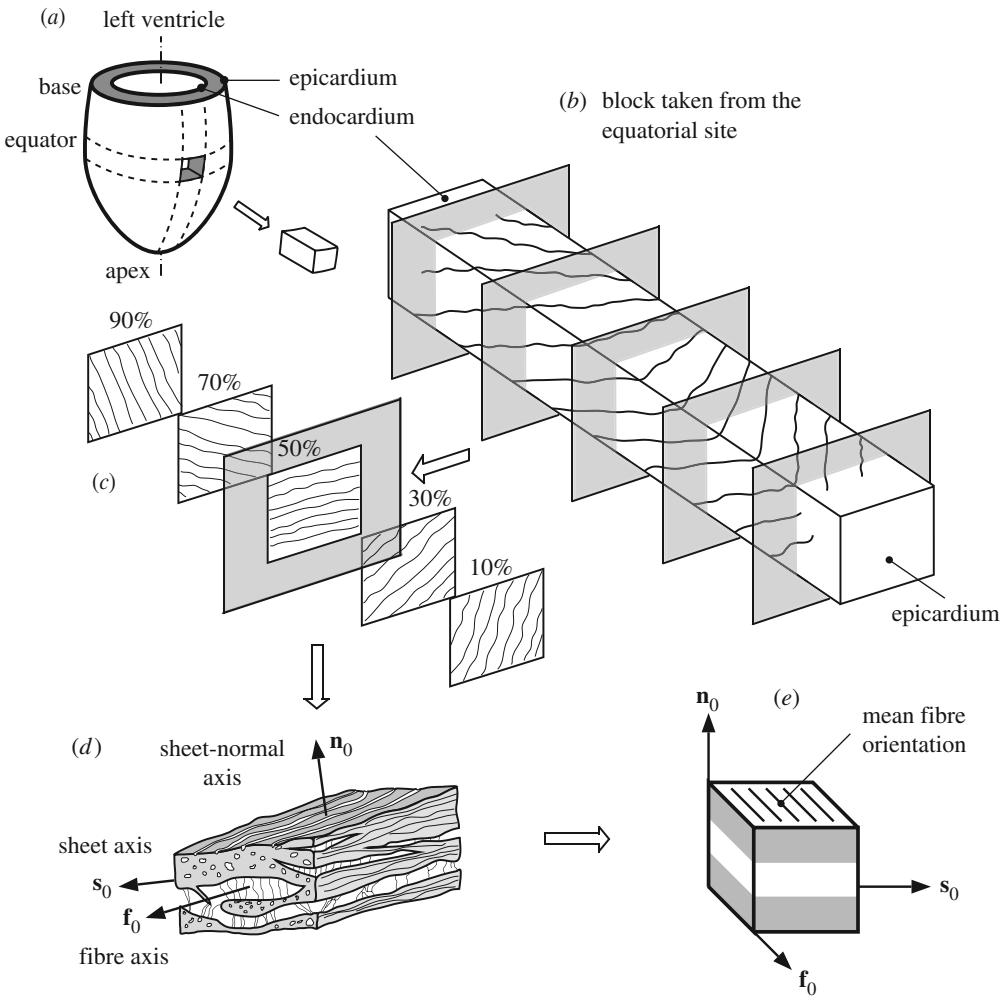

Figure 1. Schematic diagram of: (*a*) the left ventricle and a cutout from the equator; (*b*) the structure through the thickness from the epicardium to the endocardium; (*c*) five longitudinal–circumferential sections at regular intervals from 10 to 90 per cent of the wall thickness from the epicardium showing the transmural variation of layer orientation; (*d*) the layered organization of myocytes and the collagen fibres between the sheets referred to a right-handed orthonormal coordinate system with fibre axis $\mathbf{f}_0$, sheet axis $\mathbf{s}_0$ and sheet-normal axis $\mathbf{n}_0$; and (*e*) a cube of layered tissue with local material coordinates (X_1, X_2, X_3) serving as the basis for the geometrical and constitutive model.

between adjacent muscle fibres, with attachments near the z-line of the sarcomere. Figure 1*b* illustrates the change of the three-dimensional layered organization of myocytes through the wall thickness from the epicardium to the endocardium. In addition, figure 1*c* displays views of five longitudinal–circumferential sections at regular intervals through the left ventricular wall (at 10–90% of the wall thickness from the epicardium). The sections are parallel to the epicardial surface and are displayed separately in figure 1*c*. As can be seen, the muscle fibre orientations change with position through the wall; in the equatorial region, the predominant

muscle fibre direction rotates from +50° to +70° (sub-epicardial region) to nearly 0° in the mid-wall region to −50° to −70° (sub-endocardial region) with respect to the circumferential direction of the left ventricle. It should be emphasized that the layers are not, in general, parallel to the vessel walls, as can be appreciated from figure 1*b* even though it is often assumed in the literature that they are so parallel.

Figure 1*d* is a schematic of the layered organization of myocytes with a fine weave of endomysial collagen surrounding the myocytes and lateral connections, which are 120–150 nm long, between adjacent myocytes. In addition, networks of long perimysial fibres span cleavage planes and connect adjacent muscle layers, which are three or four cells thick. The perimysial fibres are most likely to be the major structural elements of the extracellular matrix. They are coiled and have a ratio of contour length to end-to-end distance of approximately 1.3 in the unloaded state of the ventricle (MacKenna *et al.* 1996). Some branching between adjacent layers is evident, although, in many instances, branching is relatively sparse, so that the inter-layer separation can be significant. Capillaries with a fairly dense and uniform distribution within the myocardial layers and on their surfaces are also present, as indicated in figure 1*d*. Understanding of the transmural variation of the myocardial tissue structure is important because this specific architecture is responsible for the resistance of the heart to bending and twisting during the cardiac cycle.

The layered organization is characterized by a right-handed orthonormal set of basis vectors and an associated orthogonal curvilinear system of coordinates. The local fixed set of (unit) basis vectors consists of the *fibre axis* $\mathbf{f}_0$, which coincides with the muscle fibre orientation, the *sheet axis* $\mathbf{s}_0$, defined to be in the plane of the layer perpendicular to the fibre direction (sometimes referred to as the cross-fibre direction), and the *sheet-normal axis* $\mathbf{n}_0$, defined to be orthogonal to the other two. Figure 1*e*, which shows a cube of layered tissue with the local material coordinates (X_1, X_2, X_3), serves as a basis for the proposed geometrical and constitutive model. In what follows we shall use the labels f, s and n to refer to fibre, sheet and normal, respectively. We shall also use the pairs fs, fn and sn to refer to the fibre-sheet, fibre-normal and sheet-normal planes, respectively.

(*b*) *Mechanical behaviour of the passive myocardium*

The passive myocardium tissue is an orthotropic material having three mutually orthogonal planes with distinct material responses, as the results of Dokos *et al.* (2002) from *simple shear* tests on passive ventricular myocardium from pig hearts clearly show. This is illustrated in figure 2, which is based on fig. 6 from the latter paper. It should be noted, however, that the ordering of the labels fn and fs in fig. 6 of Dokos *et al.* (2002) is inconsistent with the data shown in the other figures in that paper. To correct this, we have switched the roles of fs and fn in figure 2 compared with fig. 6 of Dokos *et al.* (2002). This point is discussed further in §5*d*. The tissue exhibits a regionally dependent and time-dependent, highly nonlinear behaviour with relatively low hysteresis and also directionally dependent softening as the strain increases.

From figure 2, it can be seen that ventricular myocardium is least resistant to simple shear in the fn and sn planes for shear in the f and s directions, respectively (the lowest curve in figure 2 above the positive shear axis). It is

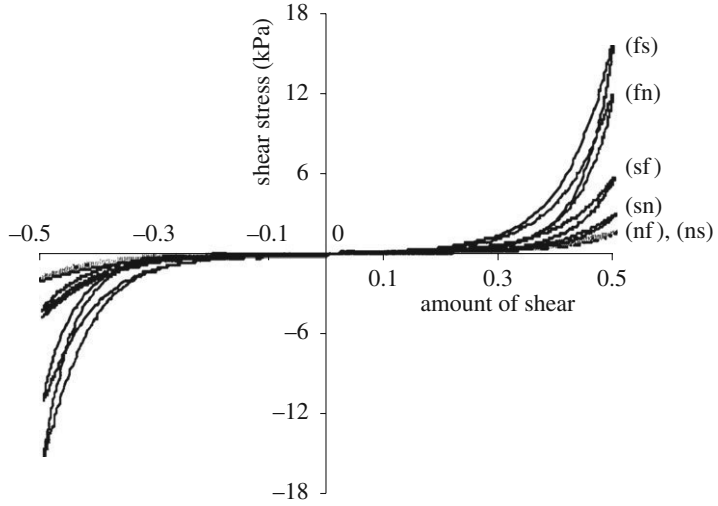

Figure 2. Shear stress versus amount of shear for simple shear tests on a cube of a typical myocardial specimen in the fs, fn and sn planes, where the (ij) shear refers to shear in the j direction in the ij plane, where $i \neq j \in \{\mathrm{f}, \mathrm{s}, \mathrm{n}\}$. Note that the (ij) shear entails stretching of material line elements that are initially in the i direction. The data show clearly the distinct responses for the three planes and hence the orthotropy of the material. In addition, it illustrates the highly nonlinear response and the viscoelastic effect evidenced by the relatively small hysteresis between loading and unloading. For the planes containing the f direction, the shear responses (fs) and (fn) in the s and n directions are different; for the planes containing the s direction, the responses (sf) and (sn) in the f and n directions are also different; the shear responses (nf) and (ns) in the planes containing the n direction are the same for the considered specimen. Adapted from Dokos *et al.* (2002).

most resistant to shear deformations that produce extension of the myocyte (f) axis in the fs and fn planes (the upper two curves for positive shear). Note, however, that for the planes containing the fibre direction, the shear responses (fs) and (fn) in the sheet and normal directions are different. Similarly, for the planes containing the sheet direction, the responses (sf) and (sn) in the fibre and normal directions are different. On the other hand, the shear responses in the planes containing the normal direction are the same for the considered specimen.

The passive *biaxial* mechanical properties of non-contracting myocardium are described by Demer & Yin (1983), Yin *et al.* (1987), Smaill & Hunter (1991) and Novak *et al.* (1994), for example. To illustrate the results, we show in figure 3 representative stress–strain data that we extracted from fig. 4 in Yin *et al.* (1987). For three different loading protocols for biaxial loading in the fs plane of a canine left ventricle myocardium, figure 3*a* shows the second Piola–Kirchhoff stress S_{ff} in the fibre direction as a function of the Green–Lagrange strain E_{ff} in the same direction, whereas figure 3*b* shows the corresponding plots for the sheet direction (S_{ss} against E_{ss}). The three sets of data in figure 3*a*,*b* correspond to constant strain ratios $E_{\mathrm{ff}}/E_{\mathrm{ss}}$. Just as for the shear response, the biaxial data indicate high nonlinearity and anisotropy. Data for unloading were not given in Yin *et al.* (1987).

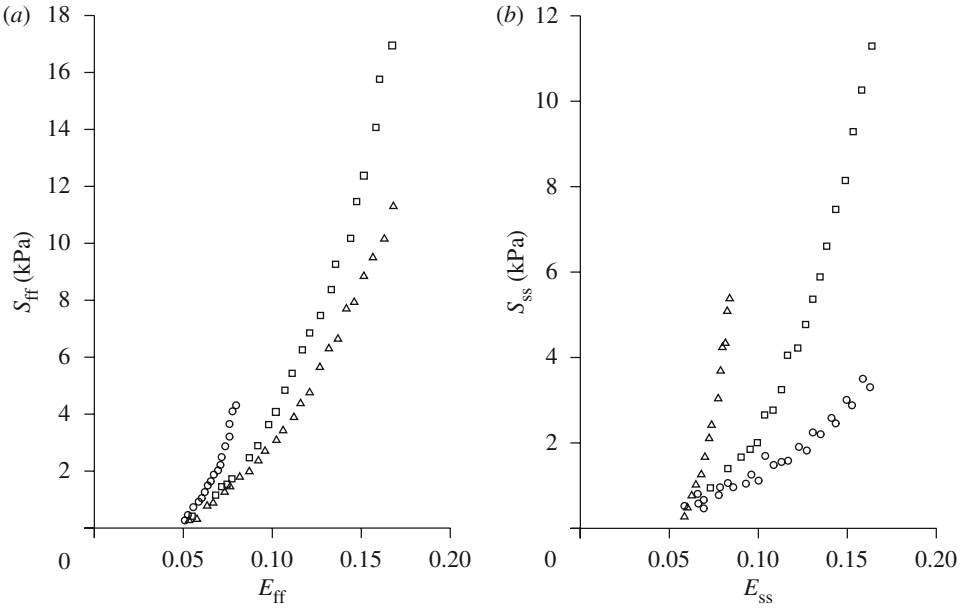

Figure 3. Representative stress–strain data for three different loading protocols for biaxial loading in the fs plane of canine left ventricle myocardium: (*a*) stress S_{ff} against strain E_{ff} in the fibre direction; (*b*) stress S_{ss} against strain E_{ss} in the sheet (cross-fibre) direction. Note that E_{ij} and S_{ij} are the components of the Green–Lagrange strain tensor and the second Piola–Kirchhoff stress tensor, respectively. The three sets of data correspond to constant strain ratios E_{ff}/E_{ss} equal to 2.05 (triangles), 1.02 (squares) and 0.48 (circles). The data are extracted from the two upper plots in fig. 4 of Yin *et al.* (1987).

As with many other soft biological tissues, the myocardium can be regarded as an incompressible material. This has been established in experiments by Vossoughi *et al.* (1980), who subjected tissue specimens to various levels of hydrostatic stress. They recorded the associated volumetric strains and concluded that the myocardial tissue is essentially incompressible.

According to experimental data obtained from equatorial slices of the left ventricular wall of potassium-arrested rat hearts, it is clear that the unloaded myocardium is residually stressed (Omens & Fung 1990) and, in particular, that there is compressive circumferential residual stress in the endocardium of the left ventricle and tensile circumferential residual stress in the epicardium; see also Costa *et al.* (1997), who suggested that the residual stress in the left ventricle is associated with pre-stretching in the plane of the myocardial sheets. According to Costa *et al.* (1997), there is relatively little residual stress along the muscle fibre direction in the mid-wall and there are also residual stresses normal to the fibre direction; the perimysial fibre network may be a primary residual stress-bearing structure in passive myocardium. Residual stresses are thought to arise during growth and remodelling (e.g. Rodriguez *et al.* 1994; Rachev 1997). Residual stresses have an important influence on the stress pattern in the typical physiological state. For example, incorporation of a residual stress distribution may reduce tensile endocardial stress concentrations predicted by

ventricular wall models (Guccione *et al.* 1991). The importance of residual stresses has also been recognized in arterial wall mechanics (e.g. Holzapfel *et al.* 2000; Holzapfel & Ogden 2003). However, three-dimensional residual stresses are very difficult to quantify and hence their modelling must be treated with caution.

Although the myocardium tissue appears to be viscoelastic, this aspect of its behaviour is not important from the point of view of mechanical modelling on the time scale of the cardiac cycle, which is short compared with the relaxation time of the viscoelastic response. Indeed, modelling of the viscoelasticity has received little attention in the literature, not least because there are very few data available on the viscoelastic properties of the tissue. An exception to this is the model of Huyghe *et al.* (1991). Here, we treat the tissue behaviour as elastic, with the characteristic features shown in figures 2 and 3.

It is therefore important to model the passive response of the left ventricular myocardium as a non-homogeneous, thick-walled, incompressible, orthotropic nonlinearly elastic material, and this is the approach we adopt in the present paper. Although residual stresses are also important for the stress analysis of the composite myocardium, it is first necessary to develop a constitutive model that takes full account of the basic structure of the material with respect to a stress-free reference configuration. Thus, we do not include residual stresses in the constitutive model developed here, as was the case for the arterial model constructed in Holzapfel *et al.* (2000).

3. Essential elements of continuum mechanics

(*a*) *Kinematical quantities and invariants*

The basic deformation variable for the description of the local kinematics is the deformation gradient $\mathbf{F}$, and we use the standard notation and convention

$$J = \det \mathbf{F} > 0. \tag{3.1}$$

For an incompressible material, we have the constraint

$$J = \det \mathbf{F} \equiv 1. \tag{3.2}$$

Associated with $\mathbf{F}$ are the right and left Cauchy–Green tensors, defined by

$$\mathbf{C} = \mathbf{F}^{\mathrm{T}}\mathbf{F} \quad \text{and} \quad \mathbf{B} = \mathbf{F}\mathbf{F}^{\mathrm{T}}, \tag{3.3}$$

respectively. Also important for what follows is the Green–Lagrange (or Green) strain tensor, defined by

$$\mathbf{E} = \tfrac{1}{2}(\mathbf{C} - \mathbf{I}), \tag{3.4}$$

where $\mathbf{I}$ is the identity tensor. The principal invariants of $\mathbf{C}$ (and also of $\mathbf{B}$) are defined by

$$I_1 = \operatorname{tr} \mathbf{C}, \quad I_2 = \tfrac{1}{2}[I_1^2 - \operatorname{tr}(\mathbf{C}^2)] \quad \text{and} \quad I_3 = \det \mathbf{C}, \tag{3.5}$$

with $I_3 = J^2 = 1$ for an incompressible material. These are *isotropic* invariants. For more details of the relevant material from continuum mechanics, we refer to Holzapfel (2000) and Ogden (1997).